

# Quantum Teleportation-Inspired Algorithm for Sampling Large Random Quantum Circuits

Ming-Cheng Chen<sup>1,2,\*</sup>, Riling Li<sup>3</sup>, Lin Gan<sup>3,4</sup>, Xiaobo Zhu<sup>1,2</sup>, Guangwen Yang<sup>3,4</sup>, Chao-Yang Lu<sup>1,2,†</sup> and Jian-Wei Pan<sup>1,2,‡</sup>

<sup>1</sup> Hefei National Laboratory for Physical Sciences at Microscale and Department of Modern Physics, University of Science and Technology of China, Hefei, Anhui 230026, China

<sup>2</sup> CAS Centre for Excellence and Synergetic Innovation Centre in Quantum Information and Quantum Physics, University of Science and Technology of China, Hefei, Anhui 230026, China.

<sup>3</sup> Department of Computer Science & Technology, Tsinghua University, Beijing, China and

<sup>4</sup> National Supercomputing Center in Wuxi, China

(Dated: January 17, 2019)

We show that low-depth random quantum circuits can be efficiently simulated by a quantum teleportation-inspired algorithm. By using logical qubits to redirect and teleport the quantum information in quantum circuits, the original circuits can be renormalized to new circuits with a smaller number of logical qubits. We demonstrate the algorithm to simulate several random quantum circuits, including 1D-chain 1000-qubit 42-depth, 2D-grid  $125 \times 8$ -qubit 42-depth and 2D-Bristlecone 72-qubit 32-depth circuits. Our results present a memory-efficient method with a clear physical picture to simulate low-depth random quantum circuits.

Information processing at quantum mechanics level has attracted great scientific interest since the development of quantum polynomial-time factoring algorithm and fault-tolerant quantum computing theory [1]. Many quantum algorithms are proposed to speed up solving important problems, such as solving linear system [2] and complex molecular structure [3]. Recently, high-fidelity quantum gates above fault-tolerance threshold have been demonstrated on superconducting qubits and trapped ions [4–6]. However, despite the great theoretical and experimental progress in the past two decades, these promising quantum algorithms still suffer from the lack of large-scale fault-tolerance quantum computing hardware or lack of strict proof of the computation complexity advantage.

The emerging quantum algorithms of Quantum Sampling open a new opportunity to demonstrate quantum computation advantage in near-term quantum computing devices [7–10]. The argument from computation complexity theory states that there is no efficient classical algorithm to simulate random quantum sampling unless the polynomial hierarchy collapses. Furthermore, the quantum sampling can be designed and implemented on near-term small-scale noisy quantum computer [11]. For examples, Boson sampling on linear optics system [7] and random quantum circuit sampling on superconducting-qubit system [12, 13] are among the most promising candidates. According to the initial estimation, about 30 single-photon boson sampling [7] or 49-qubit 40-depth 2D quantum circuit sampling [12] will be beyond the computational capabilities of the state-of-the-art supercomputers.

The classical hardness of quantum sampling in computation complexity arguments is an asymptotic statement. Exactly, how large size of quantum sampling problem will be enough to surpass classical computers is subtle [14, 15]. Recent progress in classical algorithms has refined this hardness boundary, breaking the initial 49-qubit barrier by tensor network contraction or modified Feynman-path summation methods [16–23].

In this work, we describe an efficient algorithm to calculate the probability amplitudes of low-depth random quantum circuits with a large number of qubits. The algorithm is inspired

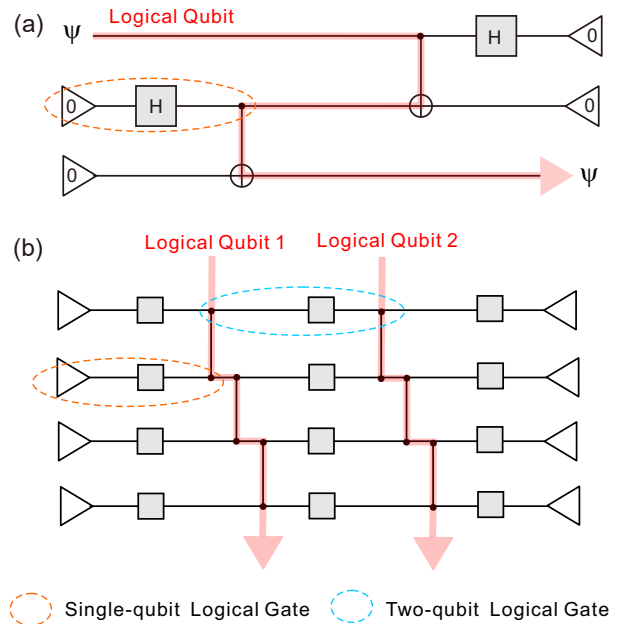


Figure 1: Quantum teleportation of multiple logical qubits for classical simulation of quantum circuits. (a) The circuit of quantum teleportation. Three physical qubits (black lines) in the quantum circuit are mimicked by one logical qubit (pink line). The logical qubit is used to redirect the flow of quantum information along the circuit topological structure. (b) The concept of transversal calculation for low-depth quantum circuits. Logical qubits are defined along the layers of two-qubit entangling gates. The number of logical qubits is proportional to the circuit depth. For a low-depth circuit, the number of logical qubits can be far less than physical qubits, therefore providing a memory-efficient classical simulation framework.

by the concept of quantum teleportation [24, 25], where quantum information can be faithfully transported along quantum entanglement. We further demonstrate the algorithm to calculate the probability amplitudes of 1000-qubit circuits and show how to efficiently generate high-fidelity samples from the calculated probability amplitudes.

Quantum-gate circuits  $U_C$  describe a sequence of quantum

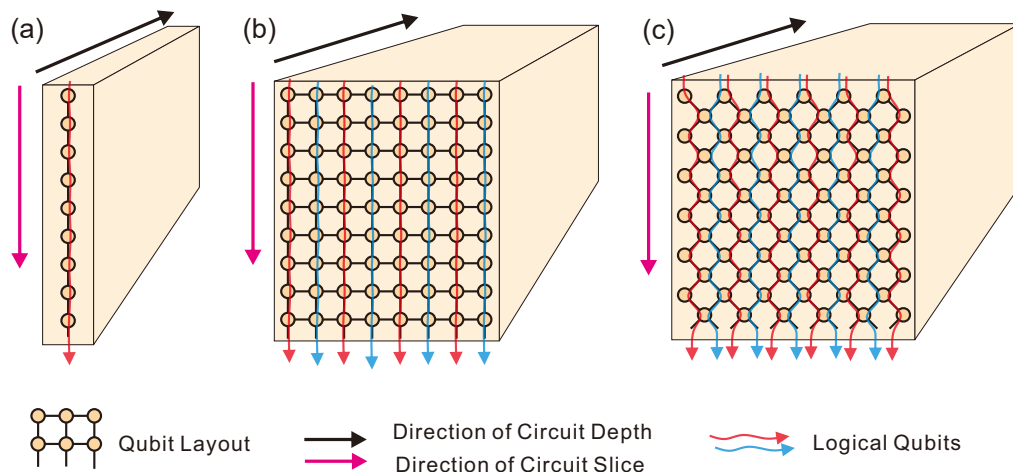


Figure 2: Examples of transversal computation. Quantum circuits are indicated by the volume of the yellow boxes. The layouts of physical qubits are shown on the surfaces of the boxes. The quantum information of the physical qubits flows along the direction of circuit depth and the quantum information of the virtual logical qubits flows along the direction of circuit slice. (a) 1D-chain 1000-qubit quantum circuit. One logical qubit is defined for every one circuit depth. (b) 2D-grid  $125 \times 8$ -qubit quantum circuit. Eight logical qubits are defined for every eight circuit depths. (c) 2D-Bristlecone  $12 \times 6$ -qubit quantum circuit. Eleven logical qubits are defined for every eight circuit depths.

operations on a multi-qubit quantum state. In the circuit, the quantum information flows from the left end to the right end. Given an input state  $|0\rangle$  and an output state  $|i\rangle$ , the circuit is equivalent to a complex number  $\langle i|U_C|0\rangle$ , called probability amplitudes. A key observation is that the circuit can also be interpreted as a quantum information network, where the lines guide the flow of information and the gate boxes represent local information operations. The lines include the world lines of physical qubits and the entangling lines of two-qubit gates. As all the lines merely represent quantum correlations, quantum information can flow along the lines at arbitrary direction. So, we can define new virtual logical qubits at some ports of the network and redirect the information flow along the lines while keeping the final probability amplitudes unchanged.

This concept is inspired from quantum teleportation protocol, as illustrated in Fig. 1(a). The original quantum teleportation circuit has three physical qubits. A new logical qubit can be defined and used to redirect the information flow along the circuit topological structure and implement the quantum information transfer.

We note that the number of virtual logical qubits can be smaller than the physical qubits. We can use this feature to renormalize a low-depth quantum circuit with large numbers of physical qubits to a new circuit with far less logical qubits. We show the basic idea in Fig. 1(b). A low-depth circuit consists of several layers of two-qubit entangling gates. Logical qubits are defined and flow transversely along these layers. The roles of world lines and entangling lines in the circuit network are exchanged, where logical qubits exist on the entangling lines and they are entangled by the world lines. Due to the number of logical qubits is proportional to the circuits depth, this method, transversal computation, implements a memory-efficient classical simulation for low-depth circuits.

The basic mathematical principle underlying the method

is that a quantum-gate circuit is translated to a tensor network and then the tensor network is translated back to a new quantum-gate circuit. That is, two different quantum-gate circuits can share the same tensor network. Examples of transformation widgets are shown in the Supplementary Materials.

Next, we demonstrate how to use transversal computation to simulate several random quantum circuits. In the first example, the qubits are arranged on a 1D chain with nearest-neighbor interaction [26, 27]. The quantum-gate circuit consists of alternating layers of random single-qubit gates and two-qubit controlled-phase (CZ) gates, as shown in Fig. 1(b) and Fig. 2(a). Logical qubits are transversely defined along the layers of entangling gates: a CZ layer (a circuit depth) has a logical qubit. Therefore, an  $N$ -qubit  $L$ -depth circuit is mapped into a new  $L$ -qubit  $N$ -depth circuit. With 1 Petabyte memory, when the depth of the original circuit is smaller than 49 [28], the new circuit can be fully stored and directly simulated by the mature technology of sparse matrix-vector multiplication.

The second example is to simulate quantum-gate circuits of 2D-grid qubits, which are proposed for quantum computational supremacy experiment with superconducting quantum circuits [12]. The qubits are arranged on the vertices of an  $M \times N$  ( $M \geq N$ ) grid. The quantum circuit consists of repetitive patterns of CZ gates, where every 8 depths of the circuit can make each pair of the nearest-neighbor qubits entangle by a single CZ gate. Meanwhile, random single-qubit gates are placed on some idle qubits in each depth. We define  $N$  logical qubits (equal to the column number  $N$ ) for every 8 circuit depths, and we transversely divided the circuit into  $M$  slices (equal to the row number  $M$ ), as shown in Fig. 2(b). The logical qubits go forward or backward on the world lines inside the slices and go across adjacent slices by the entangling lines, in the same style of the quantum teleportation circuit in Fig.

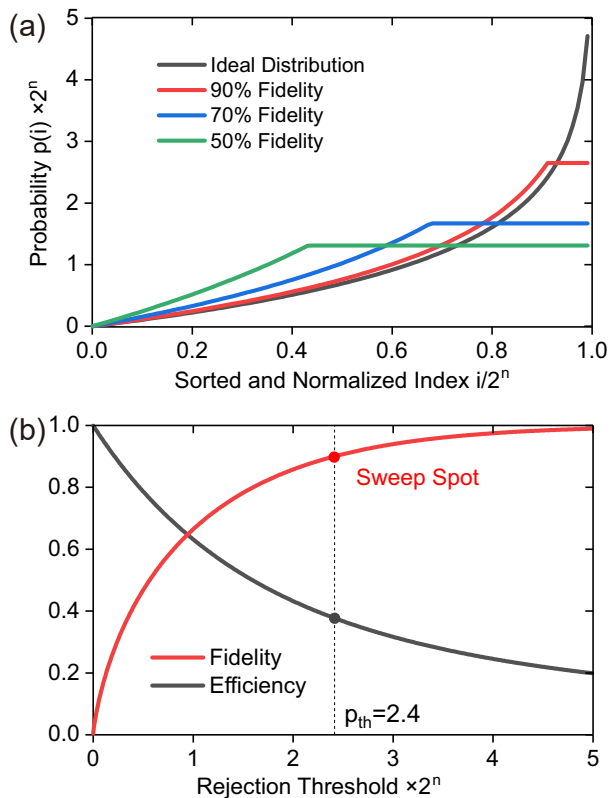


Figure 3: Threshold-rejection sampling. (a) The ideal population distribution of a random quantum state is approximated by cut-peak distributions. Approximate distributions of 0.9, 0.7 and 0.5 fidelity are shown. (b) The trade-off between sampling efficiency and sample fidelity. A sweet spot of 0.9 sample fidelity and 0.38 efficiency is shown at the threshold of  $2.4 \times 2^{-n}$ .

1(a). We show the details of each slice in the Supplementary Materials. Therefore, for  $M \times N$ -qubit  $8 \times L$ -depth circuits, the number of logical qubits is  $N \times L$ , which is smaller than the number of physical qubits when  $M > L$ .

The third example is a modified version of the above 2D layout of qubits. In the new 2D-Bristlecone layout, the qubit grid is rotated by  $45^\circ$  with a diamond boundary and the repetitive patterns of CZ gates are reordered [22]. For an  $M \times N$  ( $M \geq N$ ) grid, we define  $2N - 1$  logical qubits for every 8 circuit depths. The flow of the logical qubits is shown in Fig. 2(c) and the details of transversal circuit slices are shown in the Supplementary Materials. So, for  $M \times N$ -qubit  $8 \times L$ -depth circuits, the number of logical qubits is  $(2N - 1) \times L$ .

We simulate three circuit examples on the supercomputer Sunway TaihuLight [29]. The Sunway has 40960 computing nodes and each node has 32 Gigabytes memory and 3 TFLOPS performance. The total memory is 1.25 Petabytes, so a state vector of up to 48 logical qubits can be stored. Here, we choose to simulate 1D-chain 1000-qubit 42-depth, 2D-grid  $125 \times 8$ -qubit 42-depth and 2D-Bristlecone  $12 \times 6$ -qubit 32-depth circuits by applying 42, 40 and 44 logical qubits, respectively. As ordinary optimization methods for quantum gate circuit simulation can be directly adopted, we design a

simulator based on the evolution of wave-function according to the optimizations in [20]. The simulator uses 4096, 1024, 16384 computing nodes to produce a probability amplitude in 297.8, 131.6 and 14.1 minutes, respectively.

After the circuit simulations, we need a subsequent step to generate samples from the calculated probability amplitudes for the task of quantum circuit sampling. In general, it will consume several probability amplitudes to produce a sample. For example, Metropolis sampling using about 100 probability amplitudes [30] and frugal rejection sampling [23] using a batch of tens probability amplitudes are proposed to produce one effective sample. Here, we show that a simple threshold-rejection sampling method has a sweet spot between the sampling efficiency and the sample fidelity.

The population  $\{p(i)|i = 0, \dots, 2^n - 1\}$  of an  $n$ -qubit random quantum state obeys an exponential distribution [12]. When sorting the population in ascending order, it has function shape  $p(i) = -\ln(1 - i/2^n)/2^n$ , which has a high-and-narrow peak and a long tail. We carefully choose a threshold  $p_{th}$  to cut the distribution and get a new renormalized distribution with a flat top to approximate the ideal distribution, as shown in Fig. 3(a). Then, we use native rejection sampling to produce samples according to this new flat-top distribution by repeating the following steps: (1) suggesting a random sample  $i$  and calculate its probability  $p(i)$ ; (2) accepting the sample with a probability of  $\min(p(i)/p_{th}, 1)$ .

We show the trade-off between sampling efficiency and sample fidelity in Fig. 3(b). When setting the threshold to  $2.4 \times 2^{-n}$ , we get the sample fidelity of 0.9 with sampling efficiency of 0.38. That is, this threshold-rejection sampler can produce one statistically-independent and high-fidelity sample by consuming about 3 probability amplitudes.

Our results significantly extend both the scale and efficiency of classical simulation of random quantum sampling. We show the phase transition of classical hardness of random quantum circuits in Fig. 4. We identify an enlarged classically-easy area, where a new 49-qubit memory barrier emerges. For a quantum circuit with less than 49 logical qubits, the running time of transversal computation is proportional to the number of physical qubits, while the number of logical qubits is proportional to the circuit depth. We note that hybrid algorithms by mixing Schrodinger and Feynman methods [8] can be further used to exploit the trade-off between memory usage and running time to slightly extend the classically-easy area.

In summary, we have described a quantum teleportation-inspired algorithm to simulate low-depth random quantum circuits of a large number of qubits. The algorithm is memory-efficient and has a physically intuitive picture. Our work not only adds a new tool to efficiently simulate quantum circuits but also extend the versatile concept of quantum teleportation to enhance classical technology.

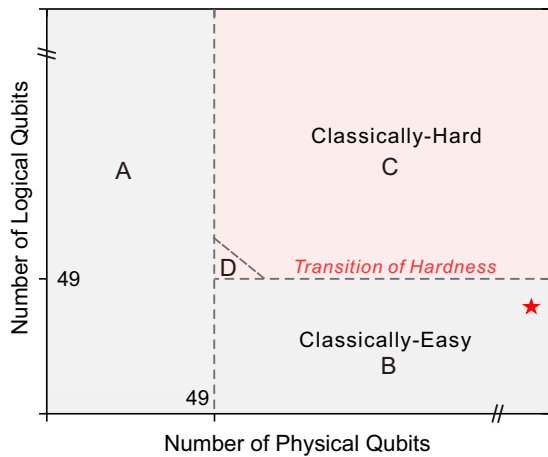


Figure 4: New 49-qubit barrier. Our memory-efficient algorithm extends the classically-easy area of sampling random quantum circuits from area A to area B, where the number of physical qubits or logical qubits (proportional to the circuit depth) can be directly stored in the state-of-the-art classical computers. The classically-hard circuits are in area C. Around the corner of area C, hybrid algorithms can exploit the trade-off between memory and runtime to slightly extend the classically-easy area to area D. The star symbol represents the 1000-qubit simulations in this work.

\* Electronic address: [cmc@ustc.edu.cn](mailto:cmc@ustc.edu.cn)

† Electronic address: [cylu@ustc.edu.cn](mailto:cylu@ustc.edu.cn)

‡ Electronic address: [pan@ustc.edu.cn](mailto:pan@ustc.edu.cn)

- [1] Nielsen, M. A. & Chuang, I. L. *Quantum Computation and Quantum Information: 10th Anniversary Edition* (Cambridge University Press, New York, NY, USA, 2011), 10th edn.
- [2] Harrow, A. W., Hassidim, A. & Lloyd, S. Quantum algorithm for linear systems of equations. *Physical review letters* **103**, 150502 (2009).
- [3] Aspuru-Guzik, A., Dutoi, A. D., Love, P. J. & Head-Gordon, M. Simulated quantum computation of molecular energies. *Science* **309**, 1704–1707 (2005).
- [4] Barends, R. *et al.* Superconducting quantum circuits at the surface code threshold for fault tolerance. *Nature* **508**, 500 (2014).
- [5] Ballance, C. J., Harty, T. P., Linke, N. M., Sepiol, M. A. & Lucas, D. M. High-fidelity quantum logic gates using trapped-ion hyperfine qubits. *Phys. Rev. Lett.* **117**, 060504 (2016).
- [6] Gaebler, J. P. *et al.* High-fidelity universal gate set for  $^9\text{Be}^+$  ion qubits. *Phys. Rev. Lett.* **117**, 060505 (2016).
- [7] Aaronson, S. & Arkhipov, A. The computational complexity of linear optics. In *Proceedings of the forty-third annual ACM symposium on Theory of computing*, 333–342 (ACM, 2011).
- [8] Aaronson, S. & Chen, L. Complexity-theoretic foundations of quantum supremacy experiments. *arXiv preprint arXiv:1612.05903* (2016).
- [9] Harrow, A. W. & Montanaro, A. Quantum computational supremacy. *Nature* **549**, 203 (2017).
- [10] Bouland, A., Fefferman, B., Nirkhe, C. & Vazirani, U. On the complexity and verification of quantum random circuit sampling. *Nature Physics* **1** (2018).
- [11] Preskill, J. Quantum computing in the nisq era and beyond. *arXiv preprint arXiv:1801.00862* (2018).
- [12] Boixo, S. *et al.* Characterizing quantum supremacy in near-term devices. *Nature Physics* **14**, 595 (2018).
- [13] Neill, C. *et al.* A blueprint for demonstrating quantum supremacy with superconducting qubits. *Science* **360**, 195–199 (2018).
- [14] Dalzell, A. M., Harrow, A. W., Koh, D. E. & La Placa, R. L. How many qubits are needed for quantum computational supremacy? *arXiv preprint arXiv:1805.05224* (2018).
- [15] Biamonte, J. D., Morales, M. E. & Koh, D. E. Quantum supremacy lower bounds by entanglement scaling. *arXiv preprint arXiv:1808.00460* (2018).
- [16] Pednault, E. *et al.* Breaking the 49-qubit barrier in the simulation of quantum circuits. *arXiv preprint arXiv:1710.05867* (2017).
- [17] Markov, I. L. & Shi, Y. Simulating quantum computation by contracting tensor networks. *SIAM Journal on Computing* **38**, 963–981 (2008).
- [18] Boixo, S., Isakov, S. V., Smelyanskiy, V. N. & Neven, H. Simulation of low-depth quantum circuits as complex undirected graphical models. *arXiv preprint arXiv:1712.05384* (2017).
- [19] Chen, Z.-Y. *et al.* 64-qubit quantum circuit simulation. *Science Bulletin* (2018).
- [20] Li, R., Wu, B., Ying, M., Sun, X. & Yang, G. Quantum supremacy circuit simulation on sunway taihulight. *arXiv preprint arXiv:1804.04797* (2018).
- [21] Chen, J., Zhang, F., Huang, C., Newman, M. & Shi, Y. Classical simulation of intermediate-size quantum circuits. *arXiv preprint arXiv:1805.01450* (2018).
- [22] Markov, I. L., Fatima, A., Isakov, S. V. & Boixo, S. Quantum supremacy is both closer and farther than it appears. *arXiv preprint arXiv:1807.10749* (2018).
- [23] Villalonga, B. *et al.* A flexible high-performance simulator for the verification and benchmarking of quantum circuits implemented on real hardware. *arXiv preprint arXiv:1811.09599* (2018).
- [24] Bennett, C. H. *et al.* Teleporting an unknown quantum state via dual classical and einstein-podolsky-rosen channels. *Physical review letters* **70**, 1895 (1993).
- [25] Raussendorf, R. & Briegel, H. J. A one-way quantum computer. *Physical Review Letters* **86**, 5188 (2001).
- [26] Emerson, J., Weinstein, Y. S., Saraceno, M., Lloyd, S. & Cory, D. G. Pseudo-random unitary operators for quantum information processing. *science* **302**, 2098–2100 (2003).
- [27] Weinstein, Y. S., Brown, W. G. & Viola, L. Parameters of pseudorandom quantum circuits. *Physical Review A* **78**, 052332 (2008).
- [28] De Raedt, H. *et al.* Massively parallel quantum computer simulator, eleven years later. *arXiv preprint arXiv:1805.04708* (2018).
- [29] Fu, H. *et al.* The sunway taihulight supercomputer: system and applications. *Science China Information Sciences* **59**, 072001 (2016).
- [30] Neville, A. *et al.* Classical boson sampling algorithms with superior performance to near-term experiments. *Nature Physics* **13**, 1153 (2017).



### Supplementary Information

**Logical gates for logical qubits.** There are two steps in transversal computation to produce a new circuit. (1) Define logical qubits along the circuit topology; (2) Translate the residual circuits between logical qubits back to logical gates. In Fig. S1, we show several basic circuit transformation widgets for the 1D circuits. For the 2D-grid (see Fig. S2) and 2D-Bristlecone (see Fig. S3) circuits, we show the details of the logical qubits in each circuit slice in Fig. S4 and Fig. S5, respectively. In Fig. S6, we show representative circuit widgets to fabricate logical gates in these new circuits.

**Sampling efficiency and sample fidelity.** The population  $\{p(i)|i = 0, \dots, 2^n - 1\}$  of a n-qubit random quantum state obeys an exponential distribution  $\text{Pr}(p) = e^{-2^n \times p}$ . When sorting the population in ascending order, the function shape is  $p(i) = -\log(1 - i/2^n)/2^n$ , as shown in Fig.

S7(a). We use a threshold  $p_{th}$  to cut the ideal (sorted) distribution  $p(i)$ , and obtain an approximate distribution  $\tilde{p}(i) = \begin{cases} \frac{-\log(1-i/2^n)/2^n}{1-e^{-p_{th}}}, & 0 \leq i < 2^n(1 - e^{-p_{th}}) \\ \frac{p_{th}}{1-e^{-p_{th}}}, & 2^n(1 - e^{-p_{th}}) \leq i < 2^n \end{cases}$ . Threshold-rejection sampling method is used to generate samples. The random suggested samples are accepted with a ratio  $A_{accept}$  and rejected with a ratio  $A_{reject}$ , as shown in Fig. S7(b). So, the sampling efficiency is  $\eta = \frac{A_{accept}}{A_{accept} + A_{reject}} = \frac{\sum_{i=0}^{2^n-1} \min(p(i), p_{th})}{2^n p_{th}}$ . The fidelity of the samples from noisy quantum state  $\rho \approx f |\psi\rangle\langle\psi| + (1 - f) \frac{I}{2^n}$  is measured by cross-entropy fidelity  $f_{CE}$ , which is equal to the quantum state fidelity  $f$ . The cross-entropy fidelity is  $f_{CE} \approx (\log 2^n + 0.577) - \sum_{i=0}^{2^n-1} \tilde{p}(i) \times \log \frac{1}{\tilde{p}(i)}$ . We use cross-entropy fidelity to characterize the effective samples generated by a threshold-rejection sampler.

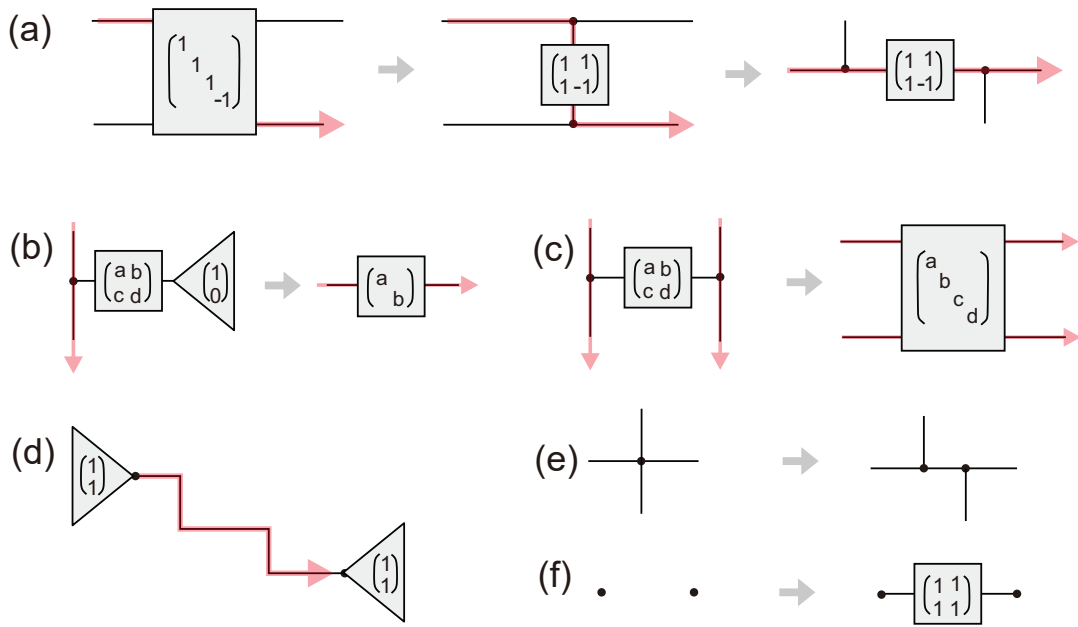


Figure S1: Basic transformation widgets. (a) A logical qubit goes through a CZ gate, accompanied by a single-qubit (non-unitary) logical gate. (b)(c) Sub-circuits in Fig. 1b in the main text are translated back to single-qubit and two-qubit logical gates. (d) Each logical qubits start from a virtual state vector  $(1, 1)^T$  and are finally projected to a virtual state vector  $(1, 1)^T$ . (e) The nodes in a circuit can be split and shifted on demand. (f) Two disconnected nodes can be connected by a line with a proper single-qubit gate.

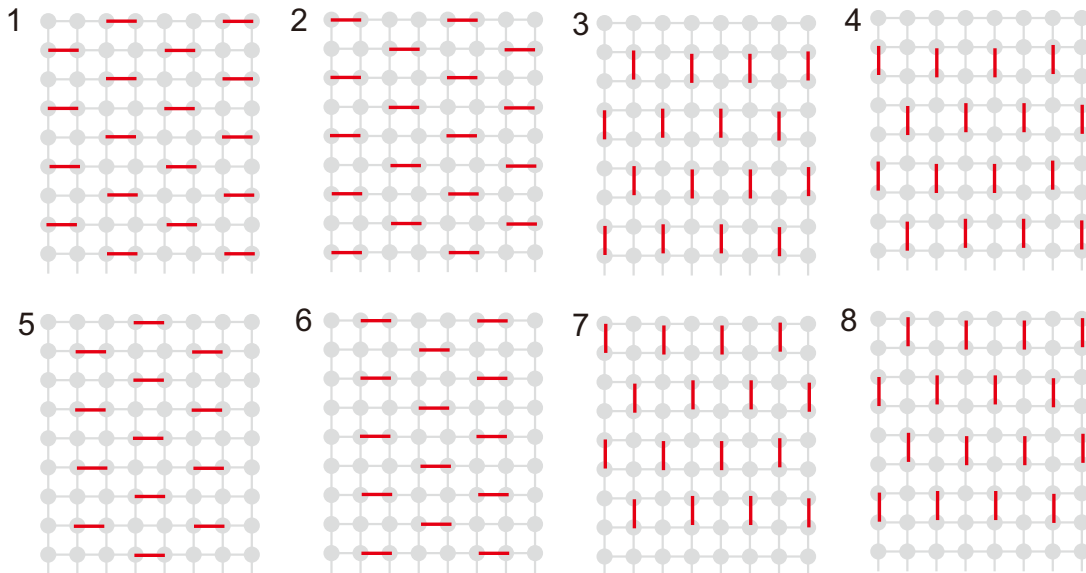


Figure S2: Layout of CZ gates for 2d-grid circuit. The circuit repeats these 8 patterns of entangling gates for every 8 circuit depths.

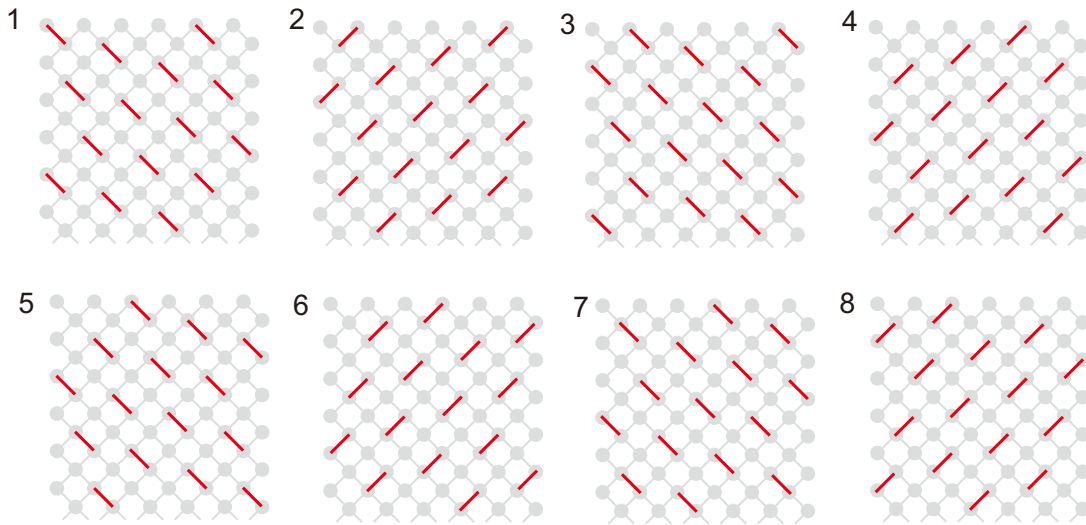


Figure S3: Layout of CZ gates for 2D-Bristlecone circuit. The circuit repeats these 8 patterns of entangling gates for every 8 circuit depths.

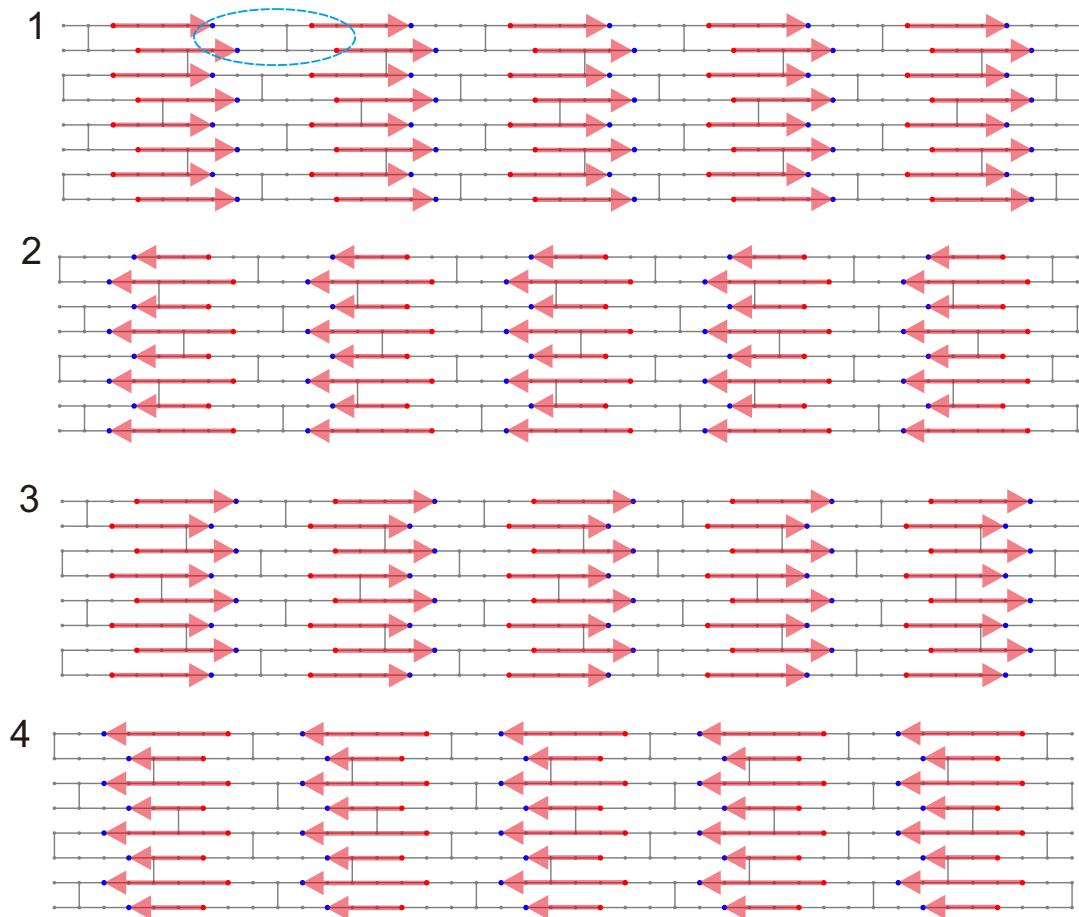


Figure S4: Layout of logical qubits: the first 4 circuit slices for 2D-grid  $125 \times 8$ -qubit 42-depth circuit. There are total 125 slices, which are the repetition of these 4 slices in order. We define 40 logical qubits, as shown in the red arrow lines. The quantum information of the logical qubits flows from one circuit slices to the next neighboring circuit slices. The entrance and exit positions (the CZ gates between two neighboring slices) for the logical qubits at each slice are shown in red and blue points, respectively. The residual circuits, the gray lines, in the slices act as multi-qubit logical gates on the logical qubits. The gray points on the lines are used to indicate the circuit depth. The complexity of transversal computation is determined by the number of logical qubits, namely, the circuit topological structure. The single-qubit gates on the circuit are not shown.

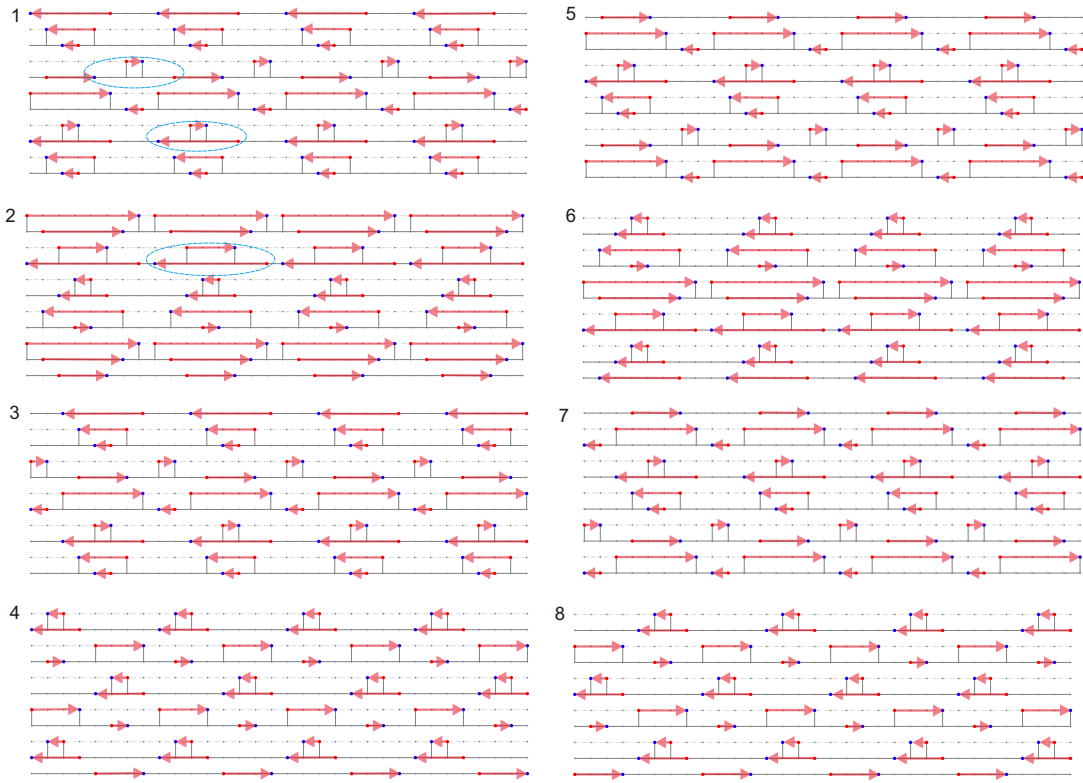


Figure S5: Layout of logical qubits: the first 8 circuit slices for 2D-Bristlecone  $12 \times 6$ -qubit 32-depth circuit. There are total 12 slices, which are the repetition of these 8 slices in order. We define 44 logical qubits, shown in the red arrow lines. The quantum information of the logical qubits flows from one circuit slices to the next neighboring circuit slices. The entrance and exit positions (the CZ gates between two neighboring slices) for the logical qubits at each slice are shown in red and blue points, respectively. The residual circuits, the gray lines, in the slices act as multi-qubit logical gates on the logical qubits. The gray points on the lines are used to indicate the circuit depth. The dashed lines are used to guide the eyes. The complexity of transversal computation is determined by the number of logical qubits, namely, the circuit topological structure. The single-qubit gates on the circuit are not shown.

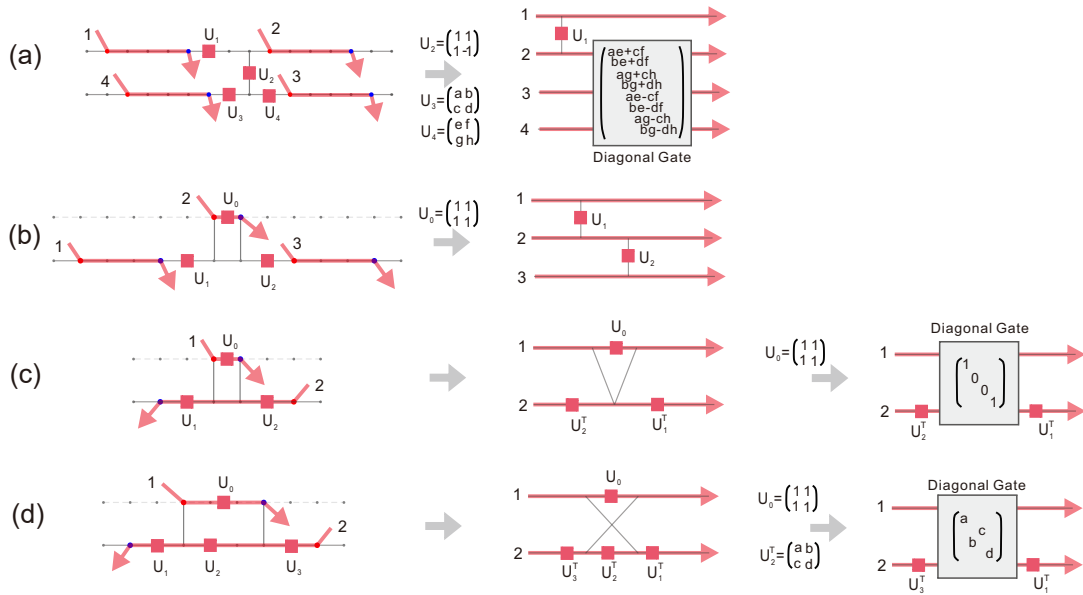


Figure S6: Logical gates. After defined the logical qubits, the residual circuits will act as logical gates on the logical qubits. We use four sub-circuits in blue cycles in Fig. S4 and Fig. S5 as examples. The single-qubit gates in the circuits are explicitly shown. We note that most of the logical gates are non-unitary diagonal gates.



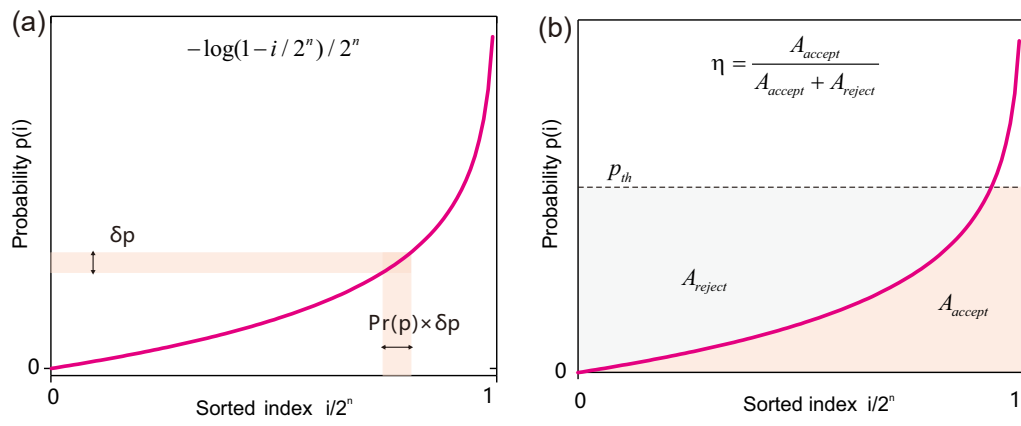


Figure S7: Threshold-rejection sampling. (a) The function of the sorted population of a random quantum state. (b) The sampling efficiency.